

Effect of strong coupling on interfacial electron transfer dynamics in dye-sensitized TiO₂ semiconductor nanoparticles

HIRENDRA N GHOSH

Radiation & Photochemistry Division, Bhabha Atomic Research Centre, Trombay, Mumbai 400 085
e-mail: hngosh@barc.gov.in

Abstract. Dynamics of interfacial electron transfer (ET) in ruthenium polypyridyl complex [*bis*-(2,2'-bpy)-(4-[2-(4'-methyl-[2,2']bipyridinyl-4-yl)-vinyl]-benzene-1,2-diol)]ruthenium(II) hexafluorophosphate (Ru-cat) and 5,10,15-*tris* phenyl-20-(3,4-dihydroxy benzene) porphyrin (TPP-cat)-sensitized TiO₂ nanoparticles have been investigated using femtosecond transient absorption spectroscopic detection in the visible and near-infrared region. We have observed that both Ru-cat and TPP-cat are coupled strongly with the TiO₂ nanoparticles through their pendant catechol moieties. We have observed a single exponential and pulse-width limited (<100 fs) electron injection from nonthermalized-excited states of Ru-complex. Here electron injection competes with the singlet–triplet manifold relaxation due to strong coupling of catecholate binding, which is a unique observation.

Optical absorption measurements indicate that the catechol moiety interacts with TiO₂ nanoparticles showing the characteristic pure catechol-TiO₂ charge-transfer (CT) band in the visible region. Transient absorption studies on TPP-cat/TiO₂ system exciting both the Soret band at 400 nm and the Q-band at 800 nm have been carried out to determine excitation wavelength-dependence on ET dynamics. The reaction channel for the electron-injection process has been found to be different for both the excitation wavelengths. Excitation at 800 nm, is found directly populate directly the excited CT state from where diffusion of electrons into the conduction band takes place. On the other hand, excitation at 400 nm light excites both the CT band of cat-TiO₂ and also Soret band of TPP-cat.

Keywords. Interfacial electron transfer dynamics; TiO₂ semiconductor nanoparticles; transient absorption spectroscopy.

1. Introduction

Relentless efforts are underway all over the world to understand the dye sensitization of wide-band gap semiconductor nanomaterials (e.g. TiO₂, SnO₂, ZnO) in view of their potential technological implication in photovoltaic energy.¹ In this area, maximum effort has been focused on dye molecules based on metal polypyridine complexes and their analogues.^{2,3} So far, *tris* bipyridyl ruthenium (II) dyes have been regarded as the best sensitizing dyes for solar energy conversion for their strong visible absorption bands, long-lived excited states and excellent photochemical stability. However, the development of organic sensitizers, which can exhibit performances similar to those of metal complexes, gained a lot of interest in the context of dye-sensitized solar cells. During the last few years, a number of organic dyes, such as phthalocyanines, tri-phenyl methane, xanthenes, coumarins, and porphyrins have been tested as sensitizers, but the light-to-electricity conversion efficiency is rather low compared to what has been

shown by metal polypyridine complexes.³ However, the metal polypyridine complexes show poor red/near-infrared light absorption. In view of the rich photochemical and electrochemical properties of porphyrins, the low cost of production and their broad absorption in the visible and NIR region, many researchers have taken keen interest in elucidating the factors, which limit their efficiency in solar cells based on dye-sensitized nanocrystalline TiO₂. High affinity for the TiO₂ surface, which is provided by the anchoring groups of the sensitizer molecules, is one of the important parameters. In most of the studies the anchoring groups of the dye molecules used in dye-sensitized solar cells including those polypyridine complexes and porphyrins are carboxylate, which bind the dye molecules with the nanoparticles. However, there are certain disadvantages in using carboxylates as anchoring groups. The ground state p*K*_a of the carboxylates is too low to ensure strong binding.⁴ Also, slow desorption of the photosensitizers can occur in the presence of water which may limit the long-term stability of the

cell. We and various other groups have observed that catechol binding is stronger than any other type of binding. Polypyridyl complexes with the pendant catechol moiety show considerable promise in the context of realizing the phenomenon of electron injection from non-thermalized states of the dye molecule. It has been suggested theoretically by Rego *et al*⁵ that, contrary to the direct charge transfer excitation in TiO₂-catechol systems, efficient photo-injection mechanisms can involve electronic excited states in the molecular adsorbate in the Ru(II)-polypyridyl-catecholate. Catechol binding with TiO₂ nanoparticles through a five-membered chelate formation is expected to be thermodynamically very stable. In our previous studies we have shown that pyrogallol red (PGR),⁶ and alizarin⁷ molecules bind strongly with TiO₂ nanoparticles through the catechol moiety and have large electronic coupling with TiO₂. In the present article we have discussed interfacial electron transfer dynamics of Ru(II)-polypyridyl-catecholate and porphyrin catechol with TiO₂ nanoparticles also to understand the influence of electronic coupling on ET dynamics using ultrafast femtosecond absorption spectroscopy.

2. Experimental

2.1 Materials

Titanium(IV) tetraisopropoxide {Ti[OCH(CH₃)₂]₄} (Aldrich, 97%), and isopropyl alcohol (Aldrich) were purified by distillation. Nanopure water (Barnsted System, USA) was used for making aqueous solutions; {*bis*-(2,2'-bpy)-(4-[2-(4'-methyl-[2,2']-bipyridinyl-4-yl)-vinyl]benzene-1,2-diol)} ruthenium(II) hexafluorophosphate ((Ru-cat) was synthesized by adopting reported procedure⁸ with some modification in the purification procedure. Synthesis of 5,10,15-*tris* phenyl-20-(3,4-dihydroxy benzene) porphyrin (TPP-cat) is reported elsewhere.⁹

2.2 Sample preparation

Nanometre-size TiO₂ was prepared by controlled hydrolysis of titanium (IV) isopropoxide and it has been described in detail in our earlier work.^{6,7}

2.3 Femtosecond visible spectrometer

The femtosecond tunable visible spectrometer (figure 1) has been developed based on a multi-pass

amplified femtosecond Ti:sapphire laser system from Avesta, Russia (1 kHz repetition rate at 800 nm, 50 fs, 800 mJ/pulse) and described earlier.⁷ The 800 nm output pulse from the multipass amplifier is split into two parts to generate pump and probe pulses. In the present investigation, we have used both 800 nm (fundamental) and its frequency doubled 400 nm as excitation sources. To generate pump pulses at 400 nm, one part of 800 nm with 200 mJ/pulse, is frequency doubled in BBO crystals. To generate visible probe pulses, about 3 mJ of the 800 nm beam is focused onto a 1.5 mm thick sapphire window. The intensity of the 800 nm beam is adjusted by iris size and ND filters to obtain a stable white light continuum in the 400 nm to over 1000 nm region. The probe pulses are split into the signal and reference beams and are detected by two matched photodiodes with variable gain. We have kept the spot sizes of the pump beam and probe beam at the crossing point around 500 and 300 micron respectively. The excitation energy density (at both 800 nm and 400 nm) was adjusted to ~2500 mJ/cm². The noise level of the white light is about ~0.5% with occasional spikes due to oscillator fluctuation. We have noticed that most laser noise is low-frequency noise and can be eliminated by comparing the adjacent probe laser pulses (pump blocked vs unblocked using a mechanical chopper). The typical noise in the measured absorbance change is about <0.3%. The instrument response function was obtained by fitting the rise time of the

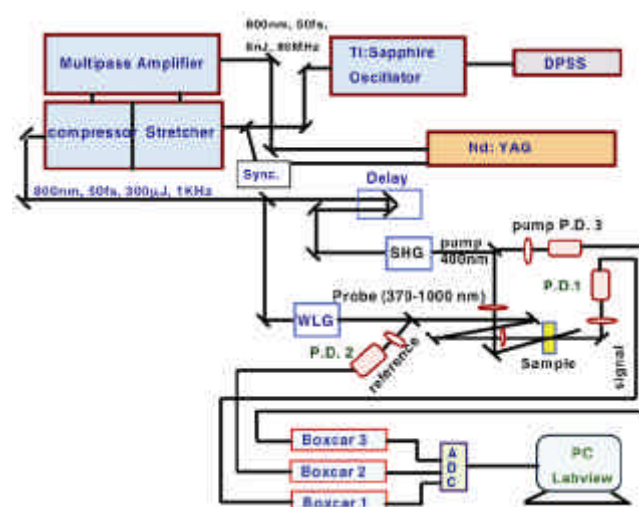


Figure 1. Molecular structure of Ru-cat and TPP-cat. Mode of interaction with TiO₂ nanoparticles through the catechol moiety.

bleach of sodium salt of *meso tetrakis* (4 sulphonatophenyl) porphyrin (TPPS) at 710 nm, which has an instantaneous response.

2.4 Cyclic voltammetry

Electrochemical experiments were performed on a CH-660A (USA) electrochemical instrument; a conventional three-electrode cell assembly was used. Oxidation redox potential of Ru-cat and TPP-cat molecule has been determined to be 1.32 V and +0.79 V against Ag/AgCl electrode respectively.

3. Results and discussion

3.1 Dye-nanoparticle interaction

The nature of the binding between a sensitizer and a semiconductor directly influences the excited-state and interfacial ET behaviour.¹⁰ Strong binding serves to anchor the sensitizer in place, control interfacial electronic coupling, and tune the redox potentials of the sensitizers and the semiconductor. However, the affinity of catechol dye molecules towards TiO₂ semiconductor nanoparticles is better as compared to the carboxylate or phosphate dye molecules, which can establish better linkage than the other two. Optical absorption studies emphasized that Ru-cat and TPP-cat interact strongly with TiO₂ nanoparticles¹¹ with the formation of a five-membered complex as shown in figure 2. Optical absorption spectrum of TPP-cat shows a Soret band with a maximum at 435 nm and a main Q-band with a maximum at 665 nm (figure 3). Steady state optical absorption measurements shows that on addition of

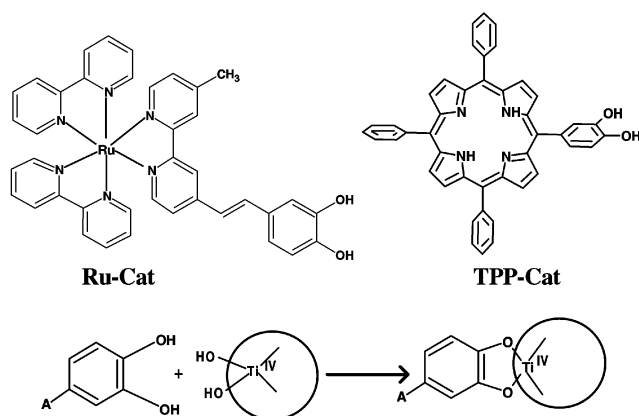


Figure 2. Schematic diagram of femtosecond transient absorption spectrometer.

TiO₂ nanoparticles, the absorption spectrum of the Q-band of TPP-cat becomes broad and shifts to longer wavelengths with increase in absorbance for the Q band at ≈ 700 nm. Red shift ≈ 40 nm (660 nm to 700 nm) and broadening of Q band of TPP-cat in presence of TiO₂ nanoparticles has been attributed to the formation of a charge transfer (CT) complex.¹² It is very interesting to observe that the Soret band of TPP-cat does not change much in presence of TiO₂ nanoparticles, however there is an increment of optical absorption in the 400–600 nm region. It that a new band appears at 400–600 nm region on top of the original Soret band. In this article we have shown that TPP-cat also interacts strongly with TiO₂ nanoparticles with the formation of a five-membered CT complex as shown in figure 1. From our measurements it is quite clear that TPP-cat molecules interact strongly with TiO₂ nanoparticles with the formation of two different types of CT complex. One CT complex (*complex 1*) is due to interaction of the catechol moiety and TiO₂ absorbing in 400–600 nm region and to the other CT complex (*complex 2*) is due to the Q-band of TPP-cat interacting with TiO₂ absorbing at the 650–900 nm region.

3.2 Steady-state emission studies in TPP-cat/TiO₂ system

We have also carried out emission measurements of freebase TPP-cat and its protonated form, as shown in figures 4a and b respectively. Freebase TPP-cat

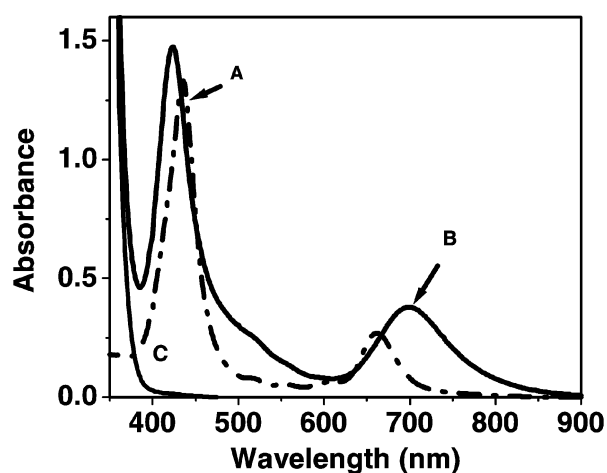


Figure 3. Optical absorption spectrum of TPP-cat in water (A), on TiO₂ nanoparticle (10 $\mu\text{g}/\text{L}$) surface (B) and the absorption spectrum of TiO₂ nanoparticle (10 $\mu\text{g}/\text{L}$) in water (C).

emits at 655 nm with a shoulder at 718 nm (figure 3a). However, the protonated form emits at single wavelength at 676 nm (figure 3b), which is located between the two emission bands (originally observed before adding acid). Our results agree well with the observations made by Akins *et al.*⁴⁷ for the case of TPP with the addition of tri-fluoro acetic acid. We have carried out steady-state emission measurements of TPP-cat both in the presence and absence of TiO₂ nanoparticles. It is observed in figure 4c that in the presence of TiO₂ nanoparticles the emission intensity decreases drastically. This is due to electron injection into the TiO₂ from the photo-excited TPP-cat molecule. However, to understand the detailed electron transfer dynamics in the TPP-cat/TiO₂ system, we have carried out ultrafast transient absorption spectroscopy.

3.3 ET dynamics in Ru-cat/TiO₂ system

We have carried out transient absorption experiments for Ru-cat-sensitized TiO₂ nanoparticles excited at 400 nm, to follow the interfacial ET dynamics on the semiconductor surface. Figure 5 shows the transient absorption spectra of Ru-cat-sensitized TiO₂ nanoparticles at different time delay. The spectrum at each time delay consists of bleach in 470–500 nm wavelength region with a maximum at ≈ 480 nm, an absorption peak at ≈ 590 nm and another broad positive absorption band in the 700–1000 nm region which has been attributed to injected electrons in the conduction band.^{6,7} The ab-

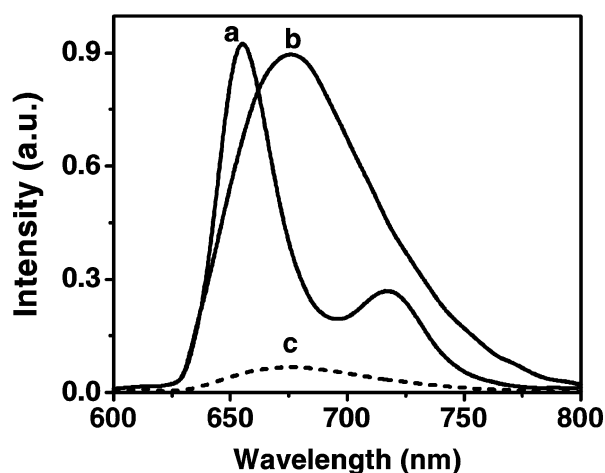


Figure 4. Steady-state emission spectra of TPP-cat in water at pH 6 (a) and pH 2.5 (b) and on TiO₂ nanoparticle (10 gm/L) surface (c).

sorption peak at 590 nm has been assigned to the Ru-cat cation radical.¹¹ Injection time in the present investigation has been determined by monitoring the appearance time of the signal of the injected electron. Figure 6 inset shows the kinetic trace of the injected electron at 900 nm. The injection time has been found to be pulse-width limited (<100 fs) and single exponential. It has been observed that the kinetic decay trace follows a multi-exponential function with time constants of 1.5 ps (34.8%), 70 ps (26.8%) and 400 ps (38.4%) that can be attributed to back electron transfer dynamics.

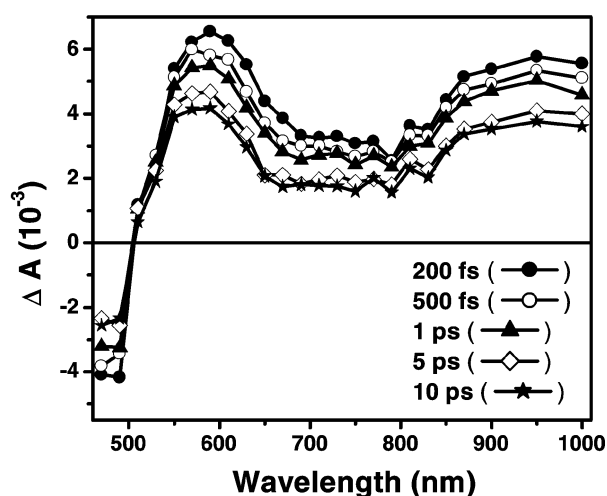


Figure 5. Transient absorption spectra of Ru-cat sensitized TiO₂ nanoparticles in water at different time delays after excitation at 400 nm.

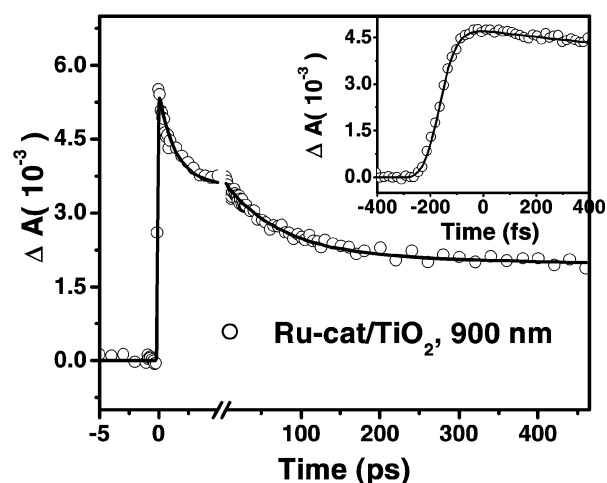
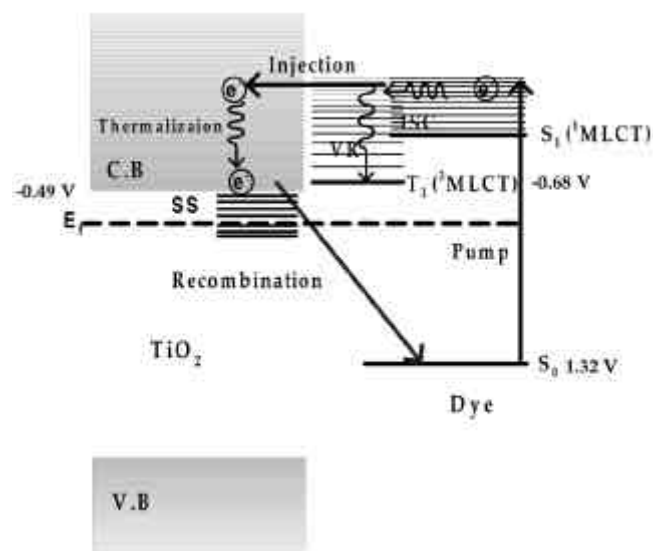


Figure 6. Kinetic decay trace of injected electrons in the conduction band at 900 nm in Ru-cat sensitized TiO₂ nanoparticles (inset shows the kinetic trace at 900 nm at shorter time scale).

Charge-transfer dynamics in Ru-(dcbpy)₂(NCS)₂ (widely known as Ru-N3) sensitized TiO₂ nanomaterials has been a subject of intense research interest for the last ten years. Much of the recent work has focused on quantifying the rate of excited-state electron injection into the semiconductor.^{13,14} In the above system, different electron-injection rates have been reported. It has been shown by femtosecond transient near IR spectroscopy that at least in some cases,¹³ injection is ultrafast and occurs prior to vibrational relaxation of the thermally equilibrated MLCT manifold, i.e., from “hot” excited states or the Frank–Condon state itself. However, most of the authors agree on the presence of sub-100 fs component and consider it to be the dominant channel with additional contributions of slower non-exponential electron injection with a distribution of characteristic times from 1 ps to tens of picoseconds. The origin of discrepancy of different electron injection dynamics is still under debate. In most of the studies it has been observed that injection dynamics is ultrafast and biphasic. Two assumptions have been made to explain the origin of the lack of single exponentiality: (i) because of the inhomogeneity of the semiconductor surface, the adsorbed dye molecules have different geometric configurations resulting different electronic coupling elements, giving rise to different rates, (ii) the fast and slow components are due to electron injection from non-thermalized ¹MLCT and thermalized ³MLCT states, respectively. However, most of researchers believe in a second hypothesis, where competition between ET from the non-thermalized states and ISC to triplet states, vibrational cooling or thermalization of triplet states is seen. Recently Bhasikuttan *et al*¹⁵ have observed that ISC process of N3 dye can be as fast as <50 fs. So it can really compete with the electron-injection process. It has been clearly demonstrated by Benko *et al*¹⁴ that electron injection in N3/TiO₂ system occurs mainly from the non-thermalized ¹MLCT state with a smaller contribution from the ³MLCT state. Most of the researchers prefer to attribute bi-phasic injection by the second mechanism as suggested above i.e., injection from ¹MLCT and ³MLCT rather than the inhomogeneities of the semiconductor surface.

One of the central points of this investigation is whether it is possible at all to observe single exponential electron injection from the photo-excited poly-pyridyl dyes to the conduction band of TiO₂ nanoparticles. The answer is affirmative, provided it

has to fulfill certain conditions. Lian and co-workers have smartly demonstrated that if the ³MLCT state of an adsorbate lies substantially below the conduction band edge then we can suppress the slow component; as a result the electron injection will be dominated by the fast component. They have observed this phenomenon in Re-carbonyl complexes (ReCO) on dry TiO₂ film,¹³ where ReCO’s relaxed excited state is estimated to be -0.35 V (SCE) lower than that of TiO₂ dry film (-0.5 V at pH 2). However, in the present investigation, the relaxed ³MLCT state of Ru-cat lies above the conduction band edge (scheme 1). So, in principle it cannot fulfill the condition, which has been demonstrated by Lian and co-workers in ReCO complexes on TiO₂ film. On the other hand, in our earlier studies, we have observed single exponential electron injection time constant in many organic dye-nanoparticle systems,^{6,7} where electron injection would only take place from the singlet excited state since the singlet–triplet ISC takes long time (>1 ns). In such systems strong electronic coupling of the dye molecules with the nanoparticles would govern the electron-injection dynamics. Strong coupling facilitates ultrafast electron injection from excited singlet state before it relaxes to the relaxed state. In the present investigation, we have observed that injection dynamics is single exponential and pulse-width limited (inset of



Scheme 1. Mechanistic scheme showing three-level model which consists of the ground state (S_0) state, the excited triplet state ($^3\text{MLCT}$) state and the excited singlet ($^1\text{MLCT}$) state of Ru(II)-polypyridyl catecholates adsorbed on TiO₂ nanoparticles.

figure 6). Even though Ru-cat complex can have both singlet ($^1\text{MLCT}$) and triplet ($^3\text{MLCT}$) manifold in the excited states, still we have observed single component in the injection kinetics. Although, it was reported earlier¹⁴ that in the Ru-polypyridyl- TiO_2 system electron injection from $^1\text{MLCT}$ (singlet) state competes with the ISC process to the $^3\text{MLCT}$ (triplet) state. In the present investigation due to very fast ISC process, non-thermalized excited states can be due to both non-thermalized $^1\text{MLCT}$ (singlet) or non-thermalized $^3\text{MLCT}$ (triplet) states or a combination of both hot singlet and triplet states (scheme 1). As a consequence of large electronic coupling in the present Ru-cat/ TiO_2 system, electron injection takes place predominantly from non-thermalized states (scheme 1) rather than from thermalized states. It is reported in the literature⁵ that on excitation of the MLCT band of Ru-polypyridyl complexes, the electron gets excited from the Ru metal centre and localized in the bi-pyridyl ligands. So it is quite obvious that on excitation with 400 nm laser light, the electron from the Ru(II) gets localized in one of the bi-pyridyl (bpy) ligands and also in the bpy-cat ligand. As bpy-cat is directly and strongly coupled with the TiO_2 nanoparticles, injection process takes place from bpy-cat ligand (TiO_2 surface-attached ligand). On the other hand, the other two bpy's are not attached directly to the nanoparticle so the de-excitation process from singlet to triplet manifold is possible. However, the redox potential of bpy-cat ligand is lower (-1.09 V) as compared to other bpy ligands (-1.19 V and -1.59 V),¹⁶ as a result upon excitation, photo-excited electron from ruthenium metal ion prefers to get localized mostly at the bpy-cat ligand, from where fast electron injection will take place due to direct coupling with the nanoparticles¹¹. As the localization takes place mostly on bpy-cat ligand, ILET process does not interfere much in the electron injection process at least for the present system. As a consequence, we have observed single exponential and pulse-width limited electron injection kinetics. On the other hand, it is very interesting to observe that recombination dynamics in Ru-cat/ TiO_2 system is faster as compared to other Ru-poly-pyridyl complex (like N3) sensitized TiO_2 nanoparticles systems.¹³ In carboxylate anchored Ru-polypyridyl complex sensitized TiO_2 system, coupling strength for ET reaction is much lower as compared to that in catechol group anchored complex. As we have observed the strong binding of the catechol group with

nanoparticles helps ultrafast single exponential injection. Similarly, it has been observed that stronger binding of catechol group also influences the BET dynamics, making it faster.

3.4 ET dynamics in TPP-cat/ TiO_2 system

One of the central themes of the present article is to understand the interfacial ET dynamics of TPP-cat/ TiO_2 system excited at 400 nm where the Soret band and CT band of catechol/ TiO_2 complex (*complex 1*) absorb, and excited at 800 nm where the CT band of *complex 2* due to interaction of Q-band and TiO_2 nanoparticles absorbs (figure 3). It is observed in figure 3 that both the CT complex of catechol/ TiO_2 and the Soret band of TPP-cat absorb at 400 nm. As a result, with 400 nm laser light we can excite both the *complex 1* and the Soret band of porphyrin molecule. Figure 7 shows that the transient spectrum at each time delay consists of an absorption peak at ≈ 610 nm, bleach in 640–750 nm wavelength region with a maximum at ≈ 700 nm, and another broad positive absorption band in 760–1000 nm region which is attributed to the conduction band electron. The absorption peak at 610 nm has been assigned to TPP-cat cation radical.¹⁷ Electron injection time (t_{inj}) has been determined by monitoring the appearance signal of the conduction band electron at 900 nm (Figure 8). We have observed that BET dynamics in TPP-cat/ TiO_2 is very fast

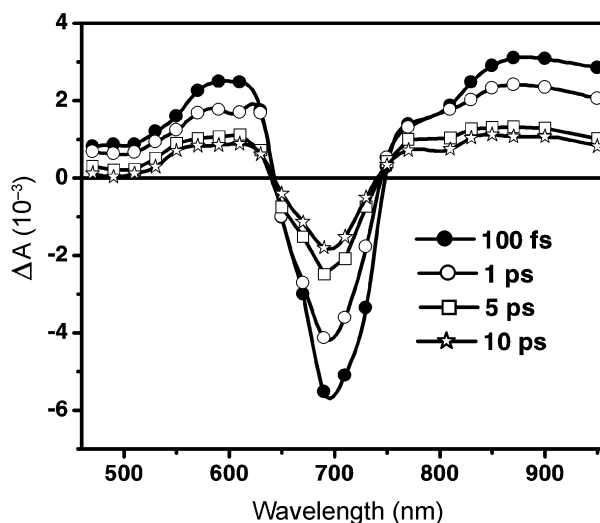


Figure 7. Transient absorption spectra of TPP-cat sensitized TiO_2 nanoparticles in water at different time delays after excitation at 400 nm.

and has been fitted with a multi-exponential function with the time constants of $t_1 = 800 \pm 70$ fs (54.9%) $t_2 = 5.3 \pm 0.5$ ps (26.4%) $t_3 = 50 \pm 2$ ps (7.7%) > 400 ps (11%). As we have attributed the 610 nm peak to the cation radical of TPP-cat, we expect that kinetic decay trace is similar to that of the conduction band electron at 900 nm. However, we have observed that kinetic decay trace at 610 nm has been best fitted with a multi-exponential function with time constants of $t_1 = 130 \pm 50$ fs (67%) $t_2 = 800 \pm 70$ fs (14.6%) $t_3 = 5.3 \pm 0.5$ ps (5.8%) $t_4 = 50 \pm 2$ ps (5.8%) $t_5 = >400$ ps (6.8%). The extra fast component (130 fs) has not been observed in other wavelengths (other than 550–610 nm region).

Figure 9 shows the transient absorption spectra of TPP-cat/TiO₂ system after excitation at 800 nm. The

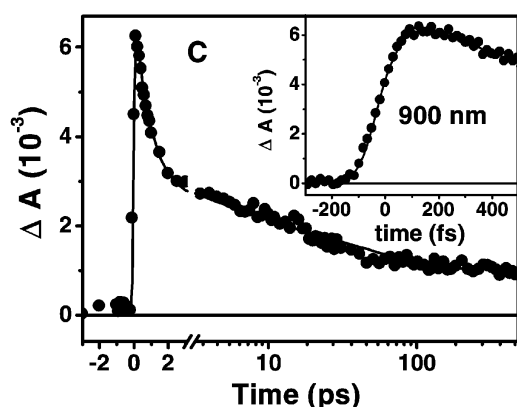


Figure 8. Kinetic decay trace of injected electrons in the conduction band at 900 nm in TPP-cat sensitized TiO₂ nanoparticles (inset shows the kinetic trace at 900 nm at shorter time scale).

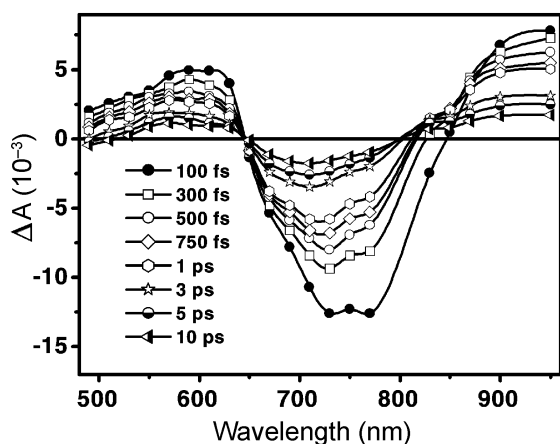


Figure 9. Transient absorption spectra of TPP-cat sensitized TiO₂ nanoparticle in water at different time delays after excitation at 800 nm.

transient spectra show a transient absorption peak at 610 nm, two bleach peaks with maxima at 770 nm and 730 nm, and broad absorption band in the 800–1000 nm region. It is interesting to see that the bleach at 770 nm recovers much faster as compared to 730 nm. We have also monitored the transient decay kinetics at 610 nm and 900 nm. Figure 10 shows the decay/recovery kinetics at different wavelengths at shorter time domain (up to 5 ps). It is seen from Figure 10 that bleach at 770 nm recovers faster as compared to that at 730 and 670 nm. However, it is interesting to see that decay dynamics at 900 nm matches fairly well with the recovery kinetics at 670 nm. We have also monitored the decay/recovery

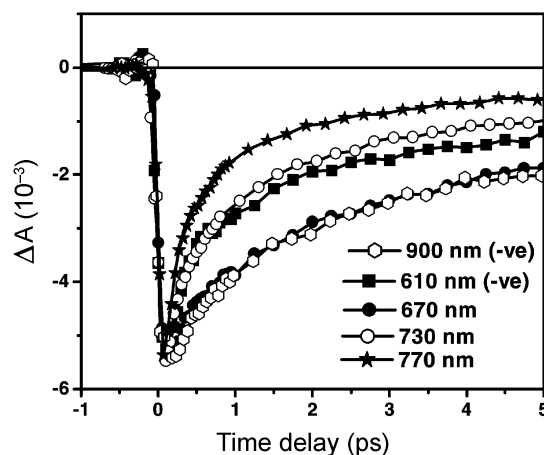


Figure 10. Kinetic decay traces at 610 nm and 900 nm and bleach recovery kinetics at 670 nm, 730 nm and 770 nm at shorter time scales (up to 5 ps) in TPP-cat sensitized TiO₂ nanoparticles after excitation at 800 nm.

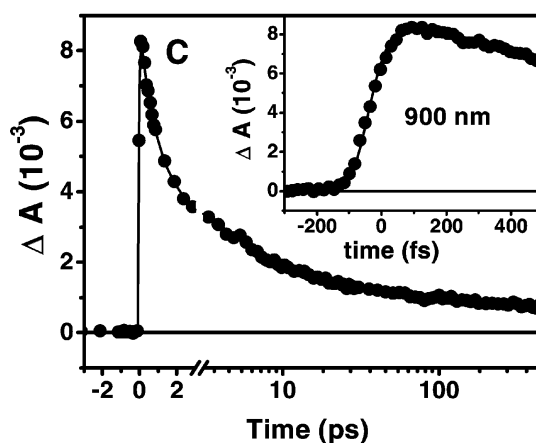


Figure 11. Kinetic decay trace of the injected electron in the conduction band at 900 nm in TPP-cat sensitized TiO₂ nanoparticles (inset shows the kinetic trace at 900 nm at shorter time scale).

Table 1. Excited state decay kinetics of TPP-cat sensitized TiO₂ nanoparticle systems at different wavelengths after exciting at 400 nm and 800 nm laser light.

Probe wavelength (nm)	Lifetimes with 400 nm excitation*	Lifetimes with 800 nm excitation*
610	$t_1 = 130 \pm 50$ (67) $t_2 = 800 \pm 70$ (14.6) $t_3 = 5.3 \pm 0.5$ (5.8) $t_4 = 50 \pm 2$ (5.8) $t_5 = > 400$ (6.8)	$t_1 = 100 \pm 50$ (64) $t_2 = 850 \pm 70$ (17.7) $t_3 = 5.1 \pm 0.5$ (12.4) $t_4 = > 400$ (5.9)
710	$t_1 = 800 \pm 70$ (54.9) $t_2 = 5.1 \pm 0.5$ (26.4) $t_3 = 50 \pm 2$ (7.7) $t_4 = > 400$ (11)	$t_1 = 100 \pm 50$ (15.5) $t_2 = 850 \pm 70$ (38.8) $t_3 = 5.3 \pm 0.5$ (36) $t_4 = > 400$ (9.7)
900	$t_1 = 800 \pm 70$ (57.3) $t_2 = 5.3 \pm 0.5$ (14) $t_3 = 50 \pm 2$ (15.3) $t_4 = > 400$ (13.4)	$t_1 = 800 \pm 70$ (44) $t_2 = 5.1 \pm 0.5$ (40.7) $t_3 = 50 \pm 5$ (3.3) $t_4 = > 400$ (12)
770		$t_1 = 100 \pm 50$ (63.6) $t_2 = 850 \pm 70$ (25.6) $t_3 = 5.3 \pm 0.5$ (7.8) $t_4 = > 400$ (3)

*Values are in femtoseconds, and numbers in parentheses are percentages

kinetics (both short time and long time) at 900 nm and have shown in figure 11. It has been observed that the decay/recovery kinetics have been fit with a multi-exponential function with different time constants (table 1). The excited state decay kinetics at 610 nm has been best fitted with time constants of $t_1 = 100 \pm 50$ fs (64%) $t_2 = 850 \pm 70$ fs (17.7%) $t_3 = 5.1 \pm 0.5$ ps (12.4%) $t_4 = > 400$ ps (5.9%). However the excited decay kinetics at 900 nm has been fit with time constants of $t_1 = 800 \pm 70$ fs (44%) $t_2 = 5.1 \pm 0.5$ ps (40.7%) $t_3 = 50 \pm 5$ ps (3.3%) $t_4 = > 400$ ps (12%). It is interesting to see that the ultrafast (~100 fs) decay component at 900 nm is absent. First of all, we will discuss the generation process of e^-_{CB} observed in near IR region. Kinetic decay trace monitored in that region (900–1000 nm) appears to have less interference from the other transient species. The processes involved in TPP-cat/TiO₂ system after excitation at 400 nm laser light are complicated as compared to 800 nm laser excitation. For the same reason, the excited state dynamics of TPP-cat/TiO₂ system after excitation at 800 nm has been discussed in advance. As mentioned earlier, a bleach at 770 nm, which corresponds to the CT band of the dye with TiO₂ nanoparticles and TPP-cat (Q-band) has been observed in the transient absorption spectra (figure 9) of TPP-cat/TiO₂ system after excitation at 800 nm, which recovers very fast

(table 1). It has also been observed that the time constant (100 fs component) for 610 nm decay kinetics match with the recovery kinetics at 770 nm (table 1). From the above observation, the excited state absorption band at 610 nm can be attributed to the excited CT band, which is a charge-separated state. The charge-separated state can return back to the ground state (*path 1*) or it can diffuse in to the conduction band (i.e. electron injection in the nanoparticles) (*path 2*) (scheme 2). The ultrafast bleach recovery at 770 nm and excited state decay kinetics at 610 nm can be ascribed to *path 1*. It is interesting to observe that the bleach at 770 nm at ~3 ps (figure 9) merges with the 710 nm bleach. Transient measurements (table 1) have shown that the lifetime of excited CT state is as short as ~100 fs. However, it is striking to see that the transient absorption at 610 nm persists even after 3 ps. This is because of the fact that the transient absorption spectra of the excited CT band and cation radical can be identical.¹⁸ The observation of excited CT state in dye-sensitized semiconductor nanoparticles seems interesting, however, this kind of observation has also been made earlier. The presence of excited CT state has been observed by Furube *et al*¹⁹ in coumarin dye (NKX-2311) sensitized ZnO nanoparticles. As a result, upon excitation of the CT band of *complex 2* by 800 nm laser light we can expect to see the excited

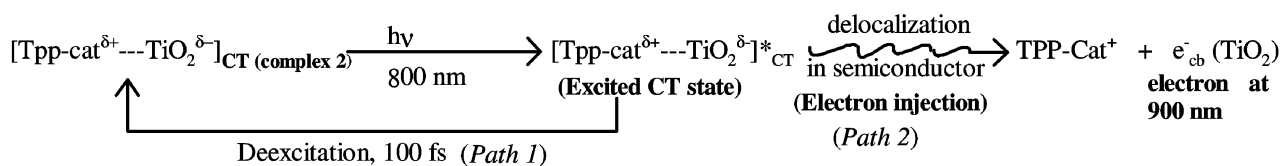
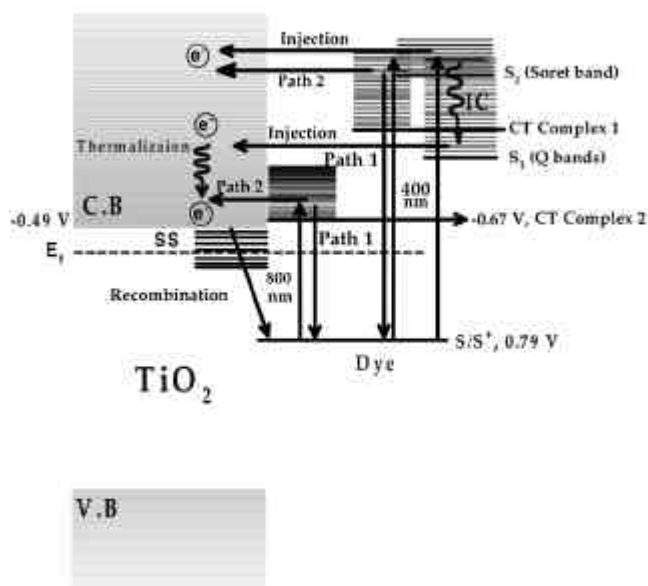


Chart 1.



Scheme 2. Mechanistic scheme showing the various processes involved in the electron-transfer dynamics of TPP-cat sensitized TiO₂ nanoparticles after excitation at 400 and 800 nm.

CT state, which is an intermediate state prior to electron injection. As the density of states in the conduction band of TiO₂ is much higher, so one could expect efficient electron injection into the conduction band of TiO₂ nanoparticles (*path 2*). However, we have observed another de-excitation channel of excited CT state to the ground state (*path 1*). The above process can be schematically represented as in chart 1.

Now, let us discuss the optical processes occurring in TPP-cat/TiO₂ system on excitation at 400 nm. It is quite clear from figure 1 that both Soret band (*S*₂) and *complex 1* have absorption at 400 nm. So on 400 nm laser excitation both the bands are excited. Energetically, Soret band is much higher as compared to that of the bottom of the conduction band edge, so thermodynamically electron injection is possible. It has been observed in porphyrin molecules that de-excitation process from Soret band (*S*₂)

to *Q* band (*S*₁) can be as fast as <10 fs²⁰ through internal conversion (IC). So the population to *Q* band is also possible, whose energy level is also higher than conduction band edge of TiO₂ (scheme 2). Hence, electron injection is also possible from *Q* band. The above process can be schematically represented in chart 2.

However, electron injection would take place only from Soret and *Q* band, and ET dynamics would have been much simpler. Decay kinetics at 610 nm (for the cation radical) would have matched with the decay kinetics at 900 nm (for *e*_{cb}⁻) and bleach recovery kinetics at 710 nm. It is seen in table 1 that decay kinetics at 900 nm matches with bleach recovery kinetics at 710 nm. However, it has been observed that decay kinetics at 610 nm is fitted with a multi-exponential function with an extra ≈100 fs time constant (table 1). Thus the excited state dynamics in TPP-cat/TiO₂ is complicated at 400 nm excitation as compared to 800 nm excitation. On exciting *complex 1* initially the hole get localized on catechol moiety which a part of TPP-cat, so it is quite obvious that the hole migrates very fast (<10 fs) to the porphyrin moiety via electron transfer from TPP. As our instrument response ≈100 fs, it is difficult to monitor the molecular process which takes place sub-10 fs. As a result, on excitation of *complex 1*, we did not observe any signature of bleach in the 400–600 nm region. The above photochemical process can be schematically represented as in chart 3.

Now from chart 2 we can explain the excitation process of *complex 1* by 400 nm excitation, the electron being localized on the Ti atom, resulting a charge-separated state. Here also the localized electron can recombine very fast (≈130 fs) with the parent TPP-cat cation (*path 1*) or it can diffuse in to the conduction band (*path 2*). The ultrafast component of the excited state decay kinetics at 610 nm can be ascribed to *path 1*.

Nonetheless, BET dynamics can be measured following bleach recovery kinetics at 710 nm or elec-

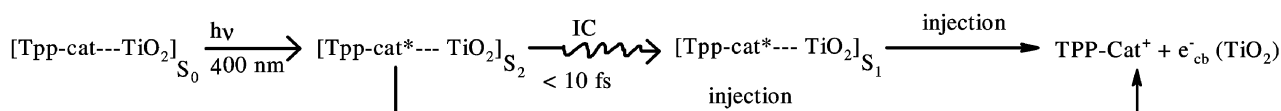


Chart 2.

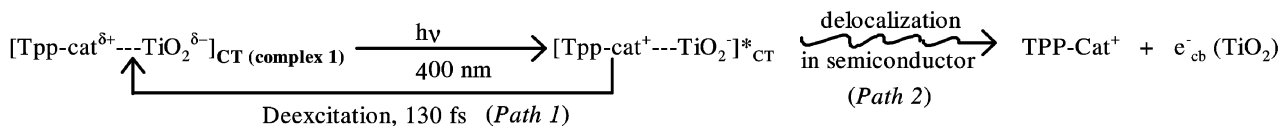


Chart 3.

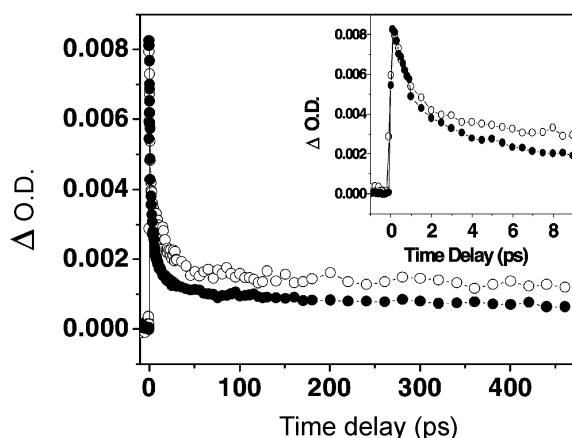


Figure 12. Comparison of charge recombination (BET) dynamics in TPP-cat sensitized TiO_2 nanoparticles monitoring injected electrons at 900 nm exciting 400 nm (○) and 800 nm (●) laser light.

tron in the conduction band at 900 nm (table 1). One of the main aims of this investigation is to study interfacial ET dynamics exciting different bands in TPP-cat/ TiO_2 system exciting 400 nm and 800 nm laser light. Figure 12 shows the comparison of BET dynamics in TPP-cat/ TiO_2 system exciting 400 nm and 800 nm laser light after monitoring the signal of conduction band electron at 900 nm. It is interesting to see that the recombination dynamics is little faster in TPP-cat/ TiO_2 system at 800 nm excitation as compared to that of at 400 nm excitation. This may be due to the fact that at 800 nm light only excites *complex 2*, where de-excitation to the ground state dominates BET dynamics due to strong coupling. On the other hand, 400 nm light excites both the Soret band and *complex 1*. On exciting the *complex 1*, both electron injection and BET process can be

faster, as we have observed on exciting *complex 2*. However, on exciting on the Soret band, electron injection can take place from both Soret and *Q* band (scheme 2). In that case, electron injection takes place through the excited state where BET dynamics is slower as compared to the complex excitation process. As a result, the net effect is that at 400 nm excitation, BET dynamics is slower as compared to that at 800 nm excitation.

4. Conclusion

Ru-cat and TPP-cat couple strongly with TiO_2 nanoparticles as the dye is absorbed on the nanoparticle surface through the pendant catechol moiety. As the $\text{p}K_a$ values for these catecholates sensitizers are as high as >9.5 , this particular dye–nanoparticle system gives greater stability even at higher pH conditions unlike other carboxylate compounds. We have studied interfacial ET dynamics in Ru-cat/ TiO_2 and TPP-cat systems using femtosecond transient absorption measurements. In Ru-cat/ TiO_2 system electron injection is found to be single exponential and pulse-width limited (<100 fs). In the present investigation electron injection process competes with thermalization process in the photo-excited state of Ru-cat. Our results indicate that electron injection take place predominantly from non-thermalized singlet state ($^1\text{MLCT}$), and/or non-thermalized triplet state ($^3\text{MLCT}$) or a combination of both, which is a unique observation in ET dynamics in Ru-poly-pyridyl/ TiO_2 systems studied so far. Strong coupling in dye–nanoparticle system facilitates ultrafast single-exponential electron injection, which competes with the thermalization process of excited states.

BET dynamics in Ru-cat/TiO₂ system have been found to be multi-exponential process with time constants of 1.5 ps (34.8%), 70 ps (26.8%), and 400 ps (38.4%).

ET dynamics in TPP-cat/TiO₂ system is complicated. Reaction channel (path) for ET processes is different for different excitation wavelengths (400 nm and 800 nm). Our studies revealed that 800 nm excitation populate the excited CT state (*complex 2*). After that it follows two different paths. *Path 1* is the photo-excited CT state which gets de-excited to the ground state with time constant ≈ 100 fs. *Path 2* is from photo-excited CT state diffusion of electrons and takes place into the conduction band of the nanoparticles, which is electron injection. On the other hand, 400 nm excitation populates the *S*₂ state (Soret band) of the porphyrin and it can relax very fast and populates the *S*₁ state (*Q*-band) and electron injection can take place from both the states. However, 400 nm laser light also excites *complex 1* where injected electrons in the Ti atom recombine very fast with the parent cation with a time scale of ≈ 130 fs (*path 1*) and also diffuse in the conduction band of TiO₂ (*path 2*). We have also observed that BET dynamics is multi-exponential in TPP-cat/TiO₂ system is faster at 800 nm light excitation as compared to that at 400 nm light excitation.

Acknowledgment

I would like to thank my co-workers Drs G Ramakrishna, D K Palit and Amitava Das (CSMCRI, Bhavnagar) for fruitful discussions. I would also like to thank Dr S K Sarkar of our Division and Dr T Mukherjee, Chemistry Group for their encouragement.

References

1. Pelizzetti M and Schiavello M 1997 *Photochemical conversion and storage of solar energy* (Dordrecht: Kluwer)
2. O'Regan B and Grätzel M 1991 *Nature (London)* **353** 737
3. Nazeeruddin M K, Pechy P, Renouard T, Zakeeruddin S M, Humphry-Baker R, Comte P, Liska P, Cevey L, Costa E, Shklover V, Spiccia L, Deacon G B, Bignozzi C A and Gratzel M 2001 *J. Am. Chem. Soc.* **123** 1613
4. Nazeeruddin M K, Zakeeruddin S M, Humphry-Baker R, Jirousek M, Liska P, Vlachopoulos N, Shklover V, Fischer C H and Gratzel M 1999 *Inorg. Chem.* **38** 6298
5. Rego G and Batista V S 2003 *J. Am. Chem. Soc.* **125** 7989
6. Ramakrishna G, Ghosh H N, Singh A K, Palit D K and Mittal J P 2001 *J. Phys. Chem.* **B105** 12786
7. Ramakrishna G, Singh A K, Palit D K and Ghosh H N 2004 *J. Phys. Chem.* **B108** 1701
8. Shukla A D, Whittl B, Bajaj H C, Das A and Ward M D 1999 *Inorg. Chim. Acta* **285** 89
9. Jose A D, Shukla A D, Krishnakumar D, Ganguly B, Das A, Ramakrishna G, Palit D K and Ghosh H N 2005 *Inorg Chem.* **44** 2414
10. Hagfeldt A and Gratzel M 1995 *Chem. Rev.* **95** 49
11. Ramakrishna G, Jose A D, Krishnakumar D, Das A, Palit D K and Ghosh H N 2005 *J. Phys. Chem.* **B109** 15445
12. Ramakrishna G, Jose A D, Krishnakumar D, Das A, Palit D K and Ghosh H N 2006 *J. Phys. Chem.* **B110** 10197
13. Asbury J B, Hao E, Wang Y Q, Ghosh H N and Lian T 2001 *J. Phys. Chem.* **B105** 4545
14. Benko G, Kallioinen J, Korppi-Tommola J E I, Yartsev A P and Sundstrom V 2002 *J. Am. Chem. Soc.* **104** 489
15. Bhasikuttan A C, Suzuki M, Nakashima S and Okada T 2002 *J. Am. Chem. Soc.* **104** 8398
16. Lee H Y, Kim Y, Dutta P K and Das A 2003 *Inorg. Chem.* **42** 4215
17. Bonnett R, Lambert C, Land E J, Scourides P A, Sinclair R S and Truscott T G 1983 *Photochem. Photobiol.* **38** 1
18. Mataga N 1991 in *Electron transfer in inorganic, organic, and biological systems* (eds) J R Bolton, N Mataga and G McLendon (Advances in Chemistry Series) (Washington, DC:) pp. 91–115
19. Furube A, Katoh R, Yoshihara T, Hara K, Murata S, Arakawa H and Tachiya M 2004 *J. Phys. Chem.* **B108** 12583
20. Zhong Q, Wang Z, Liu Y, Zhu Q and Kong F 1996 *J. Chem. Phys.* **105** 5377